Optics Letters

Experimental observation of quantum correlations in four-wave mixing with a conical pump

LEIMING CAO,[1] JINJIAN DU,[1] JINGLIANG FENG,[1] ZHONGZHONG QIN,[1] ALBERTO M. MARINO,[2] MIKHAIL I. KOLOBOV,[3,5] AND JIETAI JING[1,4,*]

[1]State Key Laboratory of Precision Spectroscopy, East China Normal University, Shanghai 200062, China
[2]Homer L. Dodge Department of Physics and Astronomy, The University of Oklahoma, 440 W. Brooks St., Norman, Oklahoma 73019, USA
[3]Université Lille, CNRS, UMR 8523—PhLAM—Physique des Lasers Atomes et Molécules, F-59000 Lille, France
[4]Collaborative Innovation Center of Extreme Optics, Shanxi University, Taiyuan, Shanxi 030006, China
[5]e-mail: Mikhai.Kolobov@univ-lille1.fr
*Corresponding author: jtjing@phy.ecnu.edu.cn

Received 1 February 2017; revised 1 March 2017; accepted 2 March 2017; posted 2 March 2017 (Doc. ID 285145); published 17 March 2017

Generation of multimode quantum states has drawn much attention recently due to its importance for both fundamental science and the future development of quantum technologies. Here, by using a four-wave mixing process with a conical pump beam, we have experimentally observed about −3.8 dB of intensity-difference squeezing between a single-axial probe beam and a conical conjugate beam. The multi-spatial-mode nature of the generated quantum-correlated beams has been shown by comparing the variation tendencies of the intensity-difference noise of the probe and conjugate beams under global attenuation and local cutting attenuation. Due to its compactness, phase-insensitive nature, and easy scalability, our scheme may find potential applications in quantum imaging, quantum information processing, and quantum metrology.

OCIS codes: (190.4380) Nonlinear optics, four-wave mixing; (270.6570) Squeezed states.

https://doi.org/10.1364/OL.42.001201

Multimode quantum states play an essential role in quantum optics and quantum information not only due to their fundamental nature [1] but also for their potential applications in quantum information processing [2]. Much effort has been made during the last decade to produce such states, and the latest achievements in photonic architectures are very promising. Various schemes have been proposed for generating continuous variable (CV), multipartite-entangled or quantum-correlated states using photonic structures, and some of them have been experimentally realized in recent years. One approach pursued in this area is to use independent, single-mode, squeezed beams generated by optical parametric oscillators (OPOs), together with multiple beam splitters to generate a CV quantum network [3]. Such a network has been experimentally realized by several groups [4–6]. Recently, several groups have experimentally followed another approach with a single multimode nonlinear process using different spatial regions of a single beam [7], multiple longitudinal [8], or temporal modes [9].

In 2007, Paul Lett's group experimentally generated a pair of intensity-correlated beams based on a nondegenerate four-wave mixing (FWM) process in a hot rubidium vapor [10]. This system has several advantages for practical implementations, e.g., no need of a cavity due to strong nonlinearity of the system, no need of phase locking due to its phase insensitive nature, and spatial separation of the generated nonclassical beams, among others. These advantages explain the rapidly growing popularity of such a system for the generation of multimode quantum states [11–20].

Due to the advantages of the FWM scheme mentioned above, it is a good candidate for generating multimode quantum states of light. In 2014, our group experimentally generated three bright strongly quantum-correlated beams by cascading two FWM processes in hot ^{85}Rb vapors [21]. After that, we achieved multiple correlated beams using the FWM process with a spatially structured pump consisting of two individual intense beams crossing at the center of a single vapor cell [22] inspired by theoretical proposals in Refs. [23,24]. Very recently, theoretical proposals based on FWM in hot ^{85}Rb were proposed to realize multipartite quantum entanglement, e.g., CV cluster state generation over a spatial comb through the FWM process in a single vapor cell [25] and versatile quantum network generation by cascading several FWM processes [26].

In Ref. [23] the authors considered the theoretical generation of tripartite entanglement in parametric down-conversion using a pump wave consisting of two tilted plane waves. Later this scheme was generalized in Ref. [24] to N pairs of symmetrically tilted plane pump waves capable of generating multipartite entanglement between $2N + 1$ spatially separated optical beams. Motivated by these theoretical results and the desire to generate ultra-large-scale multimode quantum states in the spatial domain, we use in this Letter a conical pump beam for the FWM process in a single ^{85}Rb vapor cell instead of

0146-9592/17/071201-04 Journal

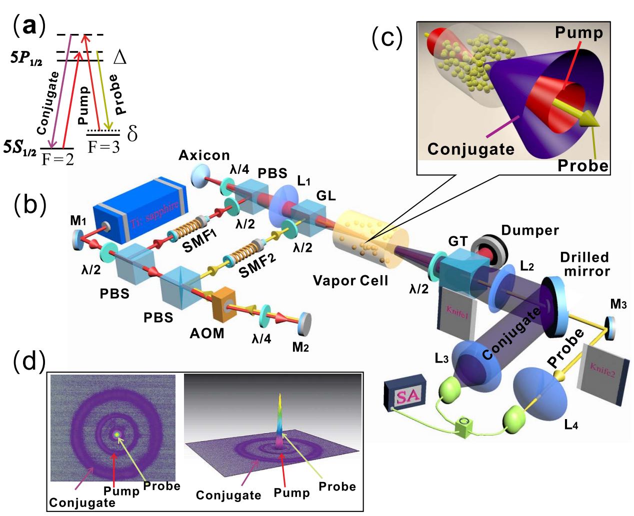

Fig. 1. Scheme for generating and detecting quantum correlated beams. (a) Double-Λ energy level diagram of the ^{85}Rb D1 line; (b) experimental layout. M1-3, high reflectivity mirrors; L1-4, lenses; Axicon, metal axicon mirror; GL, Glan–Laser polarizer; GT, Glan–Thompson polarizer; SA, spectrum analyzer. (c) Schematic of the conical-pump-based FWM. (d) Two-dimensional and three-dimensional beam pattern captured by a laser beam profiler.

a single beam or two crossing beams as in previous works [22,27,28]. Note that a conical pump beam corresponds to a continuous limit, $N \to \infty$, of N pairs of tilted plane waves, considered in Ref. [24]. The use of a conical-beam pump in the FMW leads to the generation of a probe localized around the optical axis and a conical conjugate beam with an angle of the cone twice as large as that of the pump beam. Classical parametric amplification with a conical-beam pump has been studied in the literature (see, for example, Ref. [29] and references therein). However, to the best of our knowledge, the quantum correlations between the axial probe beam and the conical conjugate beam in the FWM are experimentally demonstrated in this Letter for the first time.

We begin our experiment with a Ti:sapphire laser, and the frequency is blue detuned by about 1.2 GHz from the D1 line ($5S_{1/2}, F = 2 \to 5P_{1/2}$, 795 nm) of ^{85}Rb, which we call one-photon detuning (Δ), as shown in Fig. 1(a). The beam from the laser is split into two beams by passing through a polarizing beam splitter (PBS), as shown in Fig. 1(b). One of the beams is coupled into a single-mode fiber (SMF) in order to obtain a good Gaussian beam, and then sent to a metal axicon mirror with a conversion efficiency of about 75% to generate a conical pump beam. The half-angle of the obtained conical pump beam is about 8 mrad. The other beam goes through an acousto-optic modulator (AOM) in a double-pass configuration and then is coupled into a SMF to produce a good-shaped Gaussian beam. In this way, the probe beam, red-detuned by about 3.044 GHz from the pump, is derived, which is also 8 MHz detuned from the two-photon transition between the ground states of ^{85}Rb (hyperfine splitting of 3.036 GHz), which we call two-photon detuning (δ).

The ^{85}Rb vapor cell used in our experiment is 12.5 mm long, and the temperature is stabilized at around 120°C. It is pumped by a horizontally polarized conical beam (~210 mW) with a beam waist of 330 μm and a half-angle of 10 mrad. A vertically polarized probe beam (~40 μW) with a beam waist of 360 μm is reflected by the Glan–Laser polarizer (GL). The probe beam is injected into the vapor cell and crossed with the conical pump along the cone axis, as shown in Fig. 1(c). Due to the FWM, the probe beam is amplified with a gain of about 2.5. Amplification of the probe beam is accompanied by generation of a conical conjugate beam with a frequency of 3.044 GHz blue-shifted from the pump. The conical conjugate beam concentrically surrounds the conical pump beam due to a phase-matching condition, as shown in Fig. 1(d). The probe beam and the conical conjugate beam have powers of about 100 μW and 76 μW, respectively. We separate the amplified probe beam and the generated conical conjugate beam using a thin mirror (drilled mirror) with a circular aperture in its center. Then the probe beam and the conjugate beam are directed onto two ports of a balanced photodetector (BPD) with a gain of 10^4 V/A and a quantum efficiency of 96%. The difference of the obtained photocurrents is fed to a spectrum analyzer (SA) for data collection and analysis. The SA is set to a 30 kHz resolution bandwidth (RBW) and a 300 Hz video bandwidth (VBW). In addition, we record the noise spectra of the probe beam and the conical conjugate beam in the SA.

The experimental results of quantum correlations between the probe and the conical conjugate beams are shown in Fig. 2(a). All traces are normalized to the corresponding shot-noise limits (SNLs). The black straight line at 0 dB is taken as a reference and corresponds to the average value of the data points on the SNL (trace D). As we can see, the noise powers of the probe beam (trace A) and conjugate beam (trace B) are about 8.6 dB above the corresponding SNL, showing that they are both amplified by the FWM process. Their intensity-difference noise power (trace C) has a minimum of 3.8 dB below the corresponding SNL. This result is clear proof that we have achieved quantum correlations between a central probe beam and a conical conjugate beam. In Fig. 2(b), we show the intensity-difference noise powers of the probe and the conjugate beams at an analysis frequency of 2 MHz versus the total light power impinging on the photodetector (trace A). We do the same for the SNL (trace B). Both curves are fitted to straight lines, with a ratio of slopes equal to 0.42, indicating that the degree of intensity-difference squeezing between the probe and conical conjugate beams is about −3.8 dB.

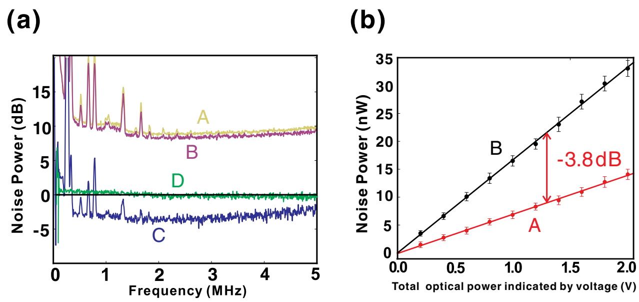

Fig. 2. Experimental results of quantum correlations. (a) Normalized noise powers of (A) probe beam, (B) conjugate beam, (C) intensity difference between the probe and the conjugate beams, (D) corresponding SNLs of trace $A \sim C$; and (b) intensity-difference noise versus total optical power indicated by voltage at 2 MHz. Red dots: FWM (trace A), black dots: SNL (trace B).

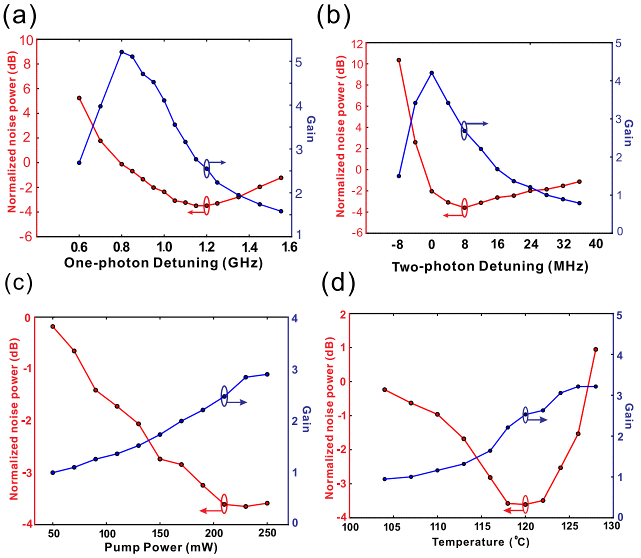

Fig. 3. Dependence of the intensity-difference squeezing and the power gain on (a) one-photon detuning; (b) two-photon detuning; (c) pump power; and (d) vapor cell temperature. The traces for the quantum correlations are plotted in red, and the traces for the power gain in blue.

We have also studied the influence of the system parameters such as one-photon detuning, two-photon detuning, pump power, and temperature of the vapor cell, on the degree of intensity-difference squeezing in our system. For simplicity, we change one parameter at a time and record the gain and the noise power of the intensity-difference between the probe and the conical conjugate beams at 2 MHz. First, we scan the one-photon detuning to study its impact. As shown in Fig. 3(a), the maximum gain is achieved at 0.8 GHz, while the maximum squeezing is at 1.2 GHz, which is larger than the corresponding value for a single FWM process used to generate quantum-correlated twin beams. As we can see, the optimal squeezing is not aligned with the maximum gain. This difference is related to an imbalance in losses between the probe and the conjugate beams. This imbalance is in part due to the fact that the probe beam is closer to resonance than the conjugate beam. As the gain increases, the noise that results from such an imbalance in losses starts to dominate and can lead to a reduction in the observed level of squeezing. Then we study the effect of two-photon detuning. As shown in Fig. 3(b), the degree of squeezing attains its optimum value between 4 and 12 MHz. There is an asymmetry in the response of the atom in terms of the two-photon detuning as explained in Ref. [30]. Such an asymmetry is responsible for efficient FWM on the positive side of the two-photon detuning but not the negative side and, as a result, on the observed level of squeezing. Next, we investigate the dependence of squeezing on the pump power. As follows from Fig. 3(c), the FWM gain grows almost linearly with the pump power below 230 mW. The degree of quantum correlation increases accordingly. However, above 230 mW, the gain is saturated, and the maximum degree of quantum correlations is −3.8 dB. Such saturation is probably due to other competing nonlinear processes. Finally, we vary the temperature of the vapor cell in order to see its influence. As shown in Fig. 3(d), the gain increases monotonously with temperature, however the optimal degree of squeezing is reached at around 120°C. As the temperature increases further, squeezing starts to deteriorate because of higher-order nonlinear effects (such as self-focusing [31]) and increasing absorption in the rubidium vapor.

So far, we have determined the optimal parameters for obtaining strong quantum correlations between the full probe and conjugate beams. However, it is more important to show the multi-spatial-mode nature of the generated quantum-correlated beams. If the generated quantum-correlated beams are not multi-spatial-mode beams, the variation tendency of the intensity-difference noise property caused by any local attenuation will exactly follow the one caused by the global attenuation of the whole beams. Of course, for all cases, both beams should be equally attenuated. In other words, if we want to claim the multi-spatial-mode nature of the generated quantum-correlated beams, we have to find a way of local-cutting attenuation causing a variation tendency of the noise property different from the one caused by global attenuation [32]. Therefore, in order to demonstrate the multi-spatial-mode nature of the generated quantum-correlated beams in our present work, we measure intensity-difference noise level of the probe and conjugate beams while equally attenuating the probe and conjugate beams in several different ways, including global attenuation of the whole beams and razor blades cutting attenuation from the same direction, opposite direction, and perpendicular direction. In each case, we record the intensity-difference noise level for different transmittance, which shows the variation tendency of the noise property.

At first we use a variable beam splitter consisting of a polarizing beam splitter and a half-wave plate to globally and equally attenuate the whole probe and conjugate beams. As shown in Fig. 4, trace A, we find that the value of the noise level is increased almost linearly to 0 as the transmittance is reduced. During the whole attenuating procedure, quantum squeezing (noise level below 0) always exists between the transmitted probe and conjugate beams.

Then we equally attenuate the probe and conjugate beams by locally cutting with razor blades from the same direction, the opposite direction, and the perpendicular

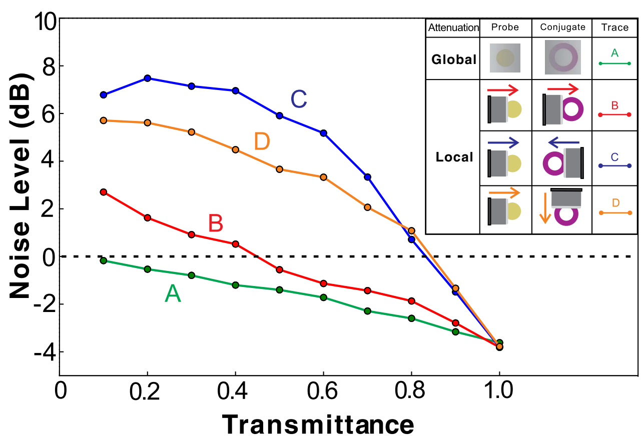

Fig. 4. Intensity difference noise levels as a function of the transmittance as the two beams are attenuated equally. Trace A, the two beams are globally attenuated with a variable beam splitter; trace $B/C/D$, the two beams are attenuated with razor blades cutting from the same direction, opposite direction, and perpendicular direction.

direction. We find that when we equally attenuate the probe and conjugate beams from the same direction, the noise level, as shown in Fig. 4, trace *B*, keeps increasing and is always higher than the one of the abovementioned global attenuation. In this case, we cut out the imperfectly correlated areas from the probe and conjugate beams and, therefore, the quantum correlation of the transmitted beams is deteriorated to some extent. However, when we equally attenuate the probe and conjugate beam from the opposite direction, the noise level increases rapidly, as shown in Fig. 4, trace *C*, and the variation tendency of the noise level is quite different from both situations of global attenuation and local cutting from the same direction. Especially, when the transmittance reduces to 0.2, the intensity-difference noise level between probe and conjugate is nearly 8 dB above the SNL, which means that almost no correlation exists between the transmitted probe and conjugate beams. In this case, we cut out the nearly uncorrelated areas from the probe and conjugate beams, so that the transmitted probe and conjugate beams are also nearly uncorrelated. Then in the case of attenuating from the perpendicular direction, we find that the variation tendency of the noise property is between the above two situations, as shown in Fig. 4, trace *D*. Therefore, we have experimentally shown that all three variation tendencies of the intensity-difference noise property caused by the three different local cutting attenuations are clearly different from the one caused by global attenuation of the whole beams. These differences undoubtedly ensure the multi-spatial-mode nature of the generated quantum-correlated beams.

In conclusion, we have experimentally demonstrated a scheme for generating quantum-correlated beams in the form of a single-axial probe beam and a conical conjugate beam using the FWM process with a conical pump in a single ^{85}Rb vapor cell. The obtained degree of intensity-difference squeezing between the probe and the conical conjugate beams is about −3.8 dB. In addition, we have investigated the influence of the system parameters, such as one-photon detuning, two-photon detuning, pump power, and temperature of the vapor cell, on the degree of intensity-difference squeezing in our system. More importantly, we have experimentally shown the multi-spatial-mode nature of the generated quantum-correlated beams. Our scheme is scalable due to its compactness and its phase insensitive nature. Our results pave the way for further research on the multimode quantum entanglement potentially present in this system. Other potential applications of spatially multimode squeezed light, such as quantum-enhanced superresolution [33] or quantum holographic teleportation [34], are still awaiting practical realization. We hope that our new scheme for generation of spatially multimode squeezed light with a conical pump will further boost development in this area.

Funding. National Natural Science Foundation of China (NSFC) (91436211, 11374104, 10974057); Program for New Century Excellent Talents in University (NCET) (NCET-10-0383); Shu Guang project (11SG26); Shanghai Pujiang Program (09PJ1404400); National Basic Research Program of China (2016YFA0302103); SRFDP (20130076110011); Program of Introducing Talents of Discipline to Universities (B12024); Natural Science Foundation of Shanghai (17ZR1442900); Program of State Key Laboratory of Advanced 207 Optical Communication Systems and Networks (2016GZKF0JT003).

REFERENCES

1. D. M. Greenberger, M. A. Horne, and A. Zeilinger, Phys. Today **46**(8), 22 (1993).
2. C. Weedbrook, S. Pirandola, R. G. Patrón, N. J. Cerf, T. C. Ralph, J. H. Shapiro, and S. Lloyd, Rev. Mod. Phys. **84**, 621 (2012).
3. P. V. Loock and S. L. Braunstein, Phys. Rev. Lett. **84**, 3482 (2000).
4. J. Jing, J. Zhang, Y. Yan, F. Zhao, C. Xie, and K. Peng, Phys. Rev. Lett. **90**, 167903 (2003).
5. H. Yonezawa, T. Aoki, and A. Furusawa, Nature **431**, 430 (2004).
6. X. Su, A. Tan, X. Jia, J. Zhang, C. Xie, and K. Peng, Phys. Rev. Lett. **98**, 070502 (2007).
7. S. Armstrong, J.-F. Morizur, J. Janousek, B. Hage, N. Treps, P. K. Lam, and H. A. Bachor, Nat. Commun. **3**, 1026 (2012).
8. M. Pysher, Y. Miwa, R. Shahrokhshahi, R. Bloomer, and O. Pfister, Phys. Rev. Lett. **107**, 030505 (2011).
9. O. Pinel, P. Jian, R. M. de Araújo, J. Feng, B. Chalopin, C. Fabre, and N. Treps, Phys. Rev. Lett. **108**, 083601 (2012).
10. C. F. McCormick, V. Boyer, E. Arimondo, and P. D. Lett, Opt. Lett. **32**, 178 (2007).
11. Q. Glorieux, L. Guidoni, S. Guibal, J. P. Likforman, and T. Coudreau, Proc. SPIE **7727**, 772703 (2010).
12. V. Boyer, A. M. Marino, R. C. Pooser, and P. D. Lett, Science **321**, 544 (2008).
13. A. M. Marino, R. C. Pooser, V. Boyer, and P. D. Lett, Nature **457**, 859 (2009).
14. J. Jing, C. Liu, Z. Zhou, Z. Y. Ou, and W. Zhang, Appl. Phys. Lett. **99**, 011110 (2011).
15. J. Kong, J. Jing, H. Wang, F. Hudelist, C. Liu, and W. Zhang, Appl. Phys. Lett. **102**, 011130 (2013).
16. F. Hudelist, J. Kong, C. Liu, J. Jing, Z. Y. Ou, and W. Zhang, Nat. Commun. **5**, 3049 (2014).
17. A. MacRae, T. Brannan, R. Achal, and A. I. Lvovsky, Phys. Rev. Lett. **109**, 033601 (2012).
18. R. C. Pooser and B. Lawrie, Optica **2**, 393 (2015).
19. A. M. Marino, V. Boyer, R. C. Pooser, P. D. Lett, K. Lemons, and K. M. Jones, Phys. Rev. Lett. **101**, 093602 (2008).
20. C. S. Embrey, M. T. Turnbull, P. G. Petrov, and V. Boyer, Phys. Rev. X **5**, 031004 (2015).
21. Z. Qin, L. Cao, H. Wang, A. M. Marino, W. Zhang, and J. Jing, Phys. Rev. Lett. **113**, 023602 (2014).
22. H. Wang, C. Fabre, and J. Jing (to be published).
23. D. Daems, F. Bernard, N. J. Cerf, and M. I. Kolobov, J. Opt. Soc. Am. B **27**, 447 (2010).
24. D. Daems and N. J. Cerf, Phys. Rev. A **82**, 032303 (2010).
25. R. Pooser and J. Jing, Phys. Rev. A **90**, 043841 (2014).
26. Y. Cai, J. Feng, H. Wang, G. Ferrini, X. Xu, J. Jing, and N. Treps, Phys. Rev. A **91**, 013843 (2015).
27. C. Liu, J. Jing, Z. Zhou, R. C. Pooser, F. Hudelist, L. Zhou, and W. Zhang, Opt. Lett. **36**, 2979 (2011).
28. Z. Qin, J. Jing, J. Zhou, C. Liu, R. C. Pooser, Z. Zhou, and W. Zhang, Opt. Lett. **37**, 3141 (2012).
29. V. Pyragaite, V. Smilgevičius, R. Butkus, A. Narmontas, A. Stabinis, and A. Piskarskas, Phys. Rev. A **90**, 023807 (2014).
30. M. T. Turnbull, P. G. Petrov, C. S. Embrey, A. M. Marino, and V. Boyer, Phys. Rev. A **88**, 033845 (2013).
31. R. W. Boyd, S. G. Lukishova, and Y. R. Shen, *Self-Focusing: Past and Present* (Springer, 2010).
32. M. Martinelli, N. Treps, S. Ducci, S. Gigan, A. Maitre, and C. Fabre, Phys. Rev. A **67**, 023808 (2014).
33. M. I. Kolobov and C. Fabre, Phys. Rev. Lett. **85**, 3789 (2000).
34. I. V. Sokolov, M. I. Kolobov, A. Gatti, and L. A. Lugiato, Opt. Commun. **193**, 175 (2001).